Original Article

Screening for biomarkers of bronchopulmonary dysplasia: a bioinformatics analysis

Xiaoqun Zhang[1,2#], Linzhou Zhu[3#], Huawei Wang[1], Jinhui Hu[1], Jie Huo[1], Shan He[1], Yueping Shen[3], Xueping Zhu[1]

[1]Department of Neonatology, Children's Hospital of Soochow University, Suzhou, China; [2]Department of Pediatrics, Affiliated Hospital of Nantong University, Nantong, China; [3]Department of Epidemiology and Biostatistics, School of Public Health, Medical College of Soochow University, Suzhou, China

Contributions: (I) Conception and design: X Zhang, Y Shen, X Zhu; (II) Administrative support: None; (III) Provision of study materials or patients: J Hu; (IV) Collection and assembly of data: L Zhu, J Huo; (V) Data analysis and interpretation: H Wang, S He; (VI) Manuscript writing: All authors; (VII) Final approval of manuscript: All authors.

[#]These authors contributed equally to this work.

Correspondence to: Xueping Zhu, PhD. Department of Neonatology, Children's Hospital of Soochow University, 92 Zhongnan Street, Industrial Park, Suzhou 215025, China. Email: zhuxueping4637@hotmail.com; Yueping Shen, PhD. Department of Epidemiology and Biostatistics, School of Public Health, Medical College of Soochow University, 199 Renai Road, Industrial Park, Suzhou 215025, China. Email: shenyueping@suda.edu.cn.

Background: Bronchopulmonary dysplasia (BPD) is a common chronic respiratory disease in preterm infants, and its incidence has gradually increased with advances in medical technology. BPD is associated with multiple complications, significantly impacting the quality of life of affected infants and imposing substantial economic burdens on families and society. Currently, the molecular mechanisms of BPD are not fully understood, and effective treatments are lacking. MicroRNAs (miRNAs), as important gene regulatory molecules, play a critical role in lung development and BPD. This study aims to investigate the potential role of miRNAs in BPD, with a particular focus on miR-9-5p and guanosine triphosphate cyclohydrolase 1 (GCH1).

Methods: Differential expression analysis of genes and miRNAs was conducted using the Gene Expression Omnibus (GEO) database. A hyperoxia-induced injury cell model was constructed to examine the expression of miR-9-5p. Target genes of miR-9-5p were predicted using online databases, followed by functional and protein interaction network analyses. In addition, cell culture, real-time quantitative polymerase chain reaction (RT-qPCR), western blotting, reactive oxygen species (ROS) level detection, malondialdehyde (MDA) assay, and Fe^{2+} detection experiments were performed.

Results: In the GSE108755 dataset, miR-9-5p was found to be upregulated in the blood of infants with BPD. In the hyperoxia-induced injury cell model, miR-9-5p expression was significantly increased. GCH1 was identified as a target gene through intersection with ferroptosis regulatory gene sets. In the cell model, GCH1 expression was markedly downregulated, while ROS, MDA, and Fe^{2+} levels were significantly elevated.

Conclusions: This study provides new insights into the molecular mechanisms of BPD, suggesting that miR-9-5p and GCH1 may serve as potential therapeutic targets for BPD. The findings contribute to a deeper understanding of the molecular basis of BPD, providing theoretical and experimental support for its diagnosis and treatment strategies. Future research will further explore the regulatory relationship between miR-9-5p and GCH1 and their roles in animal models, cell models, and clinical patients.

Keywords: Bronchopulmonary dysplasia (BPD); hyperoxia; miR-9-5p; guanosine triphosphate cyclohydrolase 1 (GCH1); ferroptosis

Submitted Dec 24, 2024. Accepted for publication Mar 25, 2025. Published online Apr 27, 2025.
doi: 10.21037/tp-2024-595
View this article at: https://dx.doi.org/10.21037/tp-2024-595

Introduction

Bronchopulmonary dysplasia (BPD) is a common and severe respiratory disease in preterm infants, with an increased incidence in infants with lower gestational age and birth weight (1). The pathological characteristics of BPD are typified by alveolar dysplasia, vascular simplification, and dysmorphic vascular development (2). In 2010, the NICHD (Eunice Kennedy Shriver National Institute of Child Health and Human Development) Neonatal Research Network reported a BPD incidence as high as 68% among preterm infants born at 22–28 weeks of gestation (3). A multicenter clinical study conducted in China in 2019 reported an incidence of BPD of 72.2% in ultra-low birth weight or extremely premature infants (4). Advances in neonatal intensive care and medical technology have also significantly improved the survival rates of extremely low and very low birth weight infants, contributing to the rising incidence of BPD (5). Premature infants with BPD show significantly higher mortality and complication rates than other preterm infants. Survivors with BPD often exhibit airway hyperresponsiveness and abnormal lung function, with frequent respiratory infections, asthma, feeding difficulties, developmental delays, and neurodevelopmental disorders during infancy and early childhood (6-8). In adulthood, they are at an elevated risk of developing chronic obstructive pulmonary disease (COPD) (9). BPD-affected children often require prolonged and recurrent hospitalizations, resulting in lifelong pulmonary impairment, significantly reduced quality of life, and heavy economic burdens on families and society (6,10). Current treatment strategies for BPD mainly include respiratory support, nutritional optimization, complication management, stem cell and gene therapy (11). However, the etiology and pathogenesis of BPD are complex, and no effective treatment is currently available. Consequently, research on the etiology, prevention, and treatment of BPD remains a priority area within the field of neonatology.

MicroRNAs (miRNAs) are highly conserved, small non-coding RNA fragments in eukaryotic cells, ranging from 18–24 nucleotides in length. They are derived from single-stranded RNA precursors processed by RNase III-type endonucleases and Dicer enzymes. miRNAs regulate protein expression by binding complementarily to the 3' end of mRNA of target genes, influencing mRNA stability and inhibiting translation (12). As key gene regulators, miRNAs control the transcription of approximately 30% of human genes (13) and play essential roles in various physiological processes, including cell differentiation, proliferation, and programmed cell death (14). Studies indicate that several miRNAs are critical in both normal and abnormal lung development, as well as in BPD (15-17). miR-9-5p plays a significant role in numerous physiological functions and is involved in the pathogenesis of multiple diseases, including various cancers (18-20) and neurological disorders (21). In pulmonary inflammation, miR-9-5p exerts protective effects in juvenile pneumonia mouse models by targeting CXCL11 and inhibiting the TLR4/NF-κB signaling pathway, thereby reducing inflammation and apoptosis (22,23). Nevertheless, no studies have yet reported on the role of miR-9-5p in BPD.

Guanosine triphosphate cyclohydrolase 1 (GCH1) is the rate-limiting enzyme in the synthesis of tetrahydrobiopterin (BH4), an essential cellular antioxidant involved in angiogenesis, inflammation, oxidative stress, and other biochemical pathways (24), which are closely associated with the pathogenesis of BPD (25). A study has shown that hyperoxia can reduce GCH1 levels in neonatal rat pups, while caffeine improves immature lungs' resistance to hyperoxic injury by increasing BH4 levels through upregulation of GCH1 and enhancement of endothelial nitric oxide synthase (eNOS) activity (26). Another study demonstrated that GCH1 overexpression could effectively prevent and mitigate radiation-induced lung injury by reducing oxidative damage from free radicals (24). However, the biological function of GCH1 in BPD remains

Highlight box

Key findings

- This study identified key genes and signaling pathways involved in bronchopulmonary dysplasia (BPD)-associated chronic respiratory disease in preterm infants utilizing bioinformatics approaches.

What is known and what is new?

- Previous studies highlighted that several miRNAs were dominant in lung development in BPD infants. However, the lack of reliable biomarkers for BPD has hampered diagnosis, prognosis, and clinical outcomes.
- The current report enhanced the pool of potential indicators by screening the differentially expressed genes and their functions in BPD infants. It underscored the role of miR-9-5p/guanosine triphosphate cyclohydrolase 1 (GCH1) and associated signaling pathways in BPD development and treatment.

What is the implication, and what should change now?

- Extra studies should be carried out to demonstrate the candidate genes and pathways in BPD progression and identify their potential as therapeutic targets.

unexplored.

Recent research has highlighted the importance of ferroptosis in BPD. Ferroptosis, a form of iron-dependent lipid peroxidation-driven cell death, is closely associated with the pathogenesis of BPD (27). It has been linked to acute lung injury in neonates (28), and evidence of ferroptosis has been observed in neonatal rat models of BPD, where inhibition of ferroptosis improved alveolar development (27,29,30). However, it remains unclear whether miRNAs play a role in BPD by regulating ferroptosis (31,32).

With advancements in gene chip technology, genomics has become widely applicable in disease research (33,34), providing extensive tools for identifying biomarkers and discovering new therapeutic targets for BPD (35-37). This study utilized the Gene Expression Omnibus (GEO) database to analyze differentially expressed miRNAs and established a hyperoxia-induced BPD cell model to examine the expression of miR-9-5p in it. The results showed that hyperoxia significantly increased miR-9-5p expression and boosted cellular damage and highlighted the pivotal function of GCH1 in the pathogenesis and management of BPD. We present this article in accordance with the MDAR reporting checklist (available at https://tp.amegroups.com/article/view/10.21037/tp-2024-595/rc).

Methods

Data acquisition and differential gene expression analysis

Using the keyword "bronchopulmonary dysplasia", a search was conducted in the GEO database (https://www.ncbi.nlm.nih.gov/geo/) with the study organism restricted to "*Homo sapiens*". The datasets GSE108755 (miRNA dataset, including five BPD samples and six normal control samples), GSE188944 (mRNA dataset, including six BPD samples and 17 control samples), and GSE108754 (mRNA dataset, including five BPD samples and six control samples) were selected. The two mRNA datasets were merged for differential analysis to obtain a set of differentially expressed genes (DEGs) for BPD. The GSE108755 dataset was normalized, and differential gene expression analysis was conducted using the limma package in R software, with significant differential miRNAs visualized in a volcano plot using the ggplot package. The fold change (FC) threshold for significant differential genes was set at $|\log FC| \geq 0.5$ and $P<0.05$. Hierarchical clustering was applied to cluster genes with similar functions, and the pheatmap package was used to display the most significantly changed miRNAs in a heatmap. The study was conducted in accordance with the Declaration of Helsinki and its subsequent amendments.

Functional analysis of DEGs

Target genes of miR-9-5p were predicted using online databases, including miRDB, miRWalk, and TargetScan8.0, and visualized through intersection analysis, resulting in 129 common predicted target genes. A Venn diagram was created using the VennDiagram package to illustrate this overlap. Functional enrichment analyses for molecular functions (MFs), cellular components (CCs), biological processes (BPs), and KEGG pathways of these 129 target genes were performed using the DAVID database (https://davidbioinformatics.nih.gov/home.jsp), with results presented in bubble plots generated using the ggplot2 package.

Protein-protein interaction (PPI) network analysis

The 129 intersecting predicted target genes were analyzed for PPI in the STRING database (http://string-db.org), extracting interaction relationships to construct a PPI network of the target gene set.

Cell culture, grouping, and intervention

MLE12 cells were obtained from Fenghui Biotechnology (CL0621, Changsha, China) and cultured in DMEM/F12 medium (10-092-CVRC, Corning, Shanghai, China) containing 10% fetal bovine serum (11011-8611-100mL, Tianhang Biotechnology, Hangzhou, China), 1% penicillin/streptomycin solution (C0224, Beyotime, Shanghai, China), and ITS culture supplement (C0341, Beyotime, Shanghai, China) at 37 ℃ in a 5% CO_2 atmosphere. Cells were seeded at a density of 2×10^5 cells per well in a six-well plate. After 24 hours of attachment, cells were divided into a control group and a hyperoxia-induced injury group (hyperoxia group). The hyperoxia group was cultured in a 37 ℃, 85% oxygen environment for 48 hours, while the control group was maintained under standard culture conditions at 37 ℃ with 5% CO_2 for 48 hours.

Real-time quantitative polymerase chain reaction (RT-qPCR) assay

The expression level of miR-9-5p was measured using RT-

Table 1 Sequences of primers

miRNAs	Sequence
miR-9-5p	AGTATGTCGATCTATTGGTTTCT
miR-15a-3p	CAGGCCATATTGTGCTGCCTCA
miR-141-3p	TAACACTGTCTGGTAAAGATGG
miR-143-3p	TGAGATGAAGCACTGTAGCTC
miR-195-5p	TAGCAGCACA GAAATATTGG C

miRNAs, microRNAs.

qPCR. Total RNA from each group of cells was extracted with TRIzol reagent (15596026, Invitrogen, Shanghai, China). Reverse transcription was performed using a specialized miRNA reverse transcription kit (638315, Takara, Dalian, China), followed by PCR amplification with a miRNA-specific real-time quantification kit (638314, Takara, Dalian, China). The reverse transcription reaction was set in a 10 µL system followed by the manufacture's guidance. The reverse transcription was carried out on a PCR instrument with incubation at 37 ℃ for 1 hour, followed by 85 ℃ for five minutes to inactivate the reverse transcriptase. Then, products of the reverse transcription were taken as templates for the following real-time PCR quantification by using a 25 µL system. The cycling protocol was as follows:

- Denaturation: 95 ℃ for 10 seconds;
- qPCR (40 cycles): 95 ℃ for five seconds, 60 ℃ for 20 seconds;
- Melt curve: 95 ℃ for 60 seconds, 55 ℃ for 30 seconds, 95 ℃ for 30 seconds.

Results were analyzed using SDS7500 software from Applied Biosystems and quantification was performed using the $2^{-\Delta\Delta Ct}$ method, with U6 RNA as the internal reference. All primers that enlisted in current study were synthesized by TaKaRa company and listed in *Table 1*.

Western blotting assay

Cells were collected, and total protein was extracted using the standard RIPA method (PO013B, Beyotime, Shanghai, China). Protein quantification was performed with a BCA Protein Quantification Kit (P0010S, Beyotime, Shanghai, China), and protein concentrations were adjusted accordingly for each group. Samples were mixed with loading buffer (P0015, Beyotime, Shanghai, China) and boiled. Sodium dodecyl sulfate-polyacrylamide gel electrophoresis (SDS-PAGE) was conducted, followed by membrane transfer onto 0.45 µm Whatman nitrocellulose membranes (10600002, MERCK, Shanghai, China). Membranes were blocked at room temperature and incubated overnight at 4 ℃ with the primary antibody (GCH1, ab307507, Abcam, Shanghai, China) at a 1:250 dilution. After washing three times with Tris-buffered saline with Tween 20 (TBST), membranes were incubated with the corresponding secondary antibody (goat anti-rabbit, A0208, Beyotime) at a 1:1,000 dilution for 3 hours at room temperature. The membranes were washed three more times with TBST, and GCH1 protein expression was detected using an ECL chemiluminescence system (P0018S, Beyotime, Shanghai, China).

ROS level detection

Cells were seeded in a six-well plate at a density of 1×10^6 cells per well and subjected to respective treatments according to the experimental groups. The DCFH-DA probe (S0035S, Beyotime, Shanghai, China) was diluted to a final concentration of 10 µmol/L in serum-free medium at a ratio of 1:1,000. After removing the cell culture medium, an appropriate volume of diluted DCFH-DA was added to each well, ensuring complete coverage of the cells (at least one milliliter per well for a six-well plate). Cells were incubated at 37 ℃ for 20 minutes in a cell incubator. After incubation, cells were washed three times with serum-free medium to remove excess DCFH-DA that had not entered the cells. Fluorescence was measured on a microplate reader with an excitation wavelength of 488 nm and an emission wavelength of 525 nm. The average fluorescence intensity of each group was calculated to reflect intracellular ROS levels. Each experiment was conducted in five times using independent cell cultures.

Malondialdehyde (MDA) assay

Cells were seeded in 10 cm dishes and treated with hyperoxia or control conditions until they reached 90% confluency. After treatment, cells were collected by trypsinization, lysed, and centrifuged at 10,000 g for 10 minutes at room temperature. The supernatant was collected, with 0.2 mL used for protein concentration measurement, while the remainder was used for MDA detection (S0131S, Beyotime, Shanghai, China). MDA working solution (200 µL) was added to each sample tube, blank tube, and standard tube according to the protocol,

followed by 100 µL of the test sample, standard, or control. The mixture was incubated in a 100 ℃ water bath for 15 minutes, then cooled in a water bath. Absorbance at 532 nm was measured in a 96-well plate, and MDA content was calculated.

Ferrous ion detection in cells

The assay was performed according to the kit instructions (E-BC-K881-M, Elabscience, Wuhan, China), as outlined below: collected cells were lysed by adding 0.2 mL of reagent I per 1×10^6 cells, mixed thoroughly, and placed on ice for 10 minutes. The lysate was then centrifuged at 15,000 ×g for 10 minutes, and the supernatant was collected. A standard curve solution with varying concentrations of ferrous ions, as well as test and control solutions, was prepared. For the assay, 80 µL of reagent II was added to the control wells, and 80 µL of reagent III was added to the test and standard wells. After mixing, the plate was incubated at 37 ℃ for 10 minutes. Optical density (OD) values for each well were measured at 593 nm on a microplate reader.

Statistical analysis

Statistical analysis was conducted using SPSS 23.0 and GraphPad Prism 8.0 software. For data with normal or approximately normal distributions, results were expressed as mean ± standard deviation, and comparisons between two groups were made using an independent sample *t*-test. For data with skewed distributions, results were expressed as median (interquartile range), and comparisons between two groups were made using the Mann-Whitney *U* test. Categorical data were described using frequency and composition ratios, with comparisons between groups made using the non-parametric χ^2 test. A significance level of α=0.05 was used, and P values were two-sided, with P<0.05 considered statistically significant.

Results

Identification of DEGs in BPD

To obtain a set of DEGs for BPD, we collected and annotated a substantial amount of relevant data from the GEO database to obtain a set of DEGs for BPD. The datasets GSE188944 and GSE108754 were employed for the screening of DEGs associated with BPD. The identification of 475 genes was based on the criteria of |logFC| >1 and P<0.05, resulting in the classification of 283 genes as upregulated and 192 genes as downregulated (*Figure 1A,1B*). The Gene Ontology (GO) enrichment method is frequently employed to elucidate the relationships between genes and GO terms, whereas the Kyoto Encyclopedia of Genes and Genomes (KEGG) enrichment method can be utilized to identify gene-pathway correlations. The three ontologies in the GO enrichment analysis are "BP" (*Figure 1C*), "CC" (*Figure 1D*), and "MF" (*Figure 1E*). Specifically, the DEGs were significantly enriched in cell adhesion and signal transduction (BP), and in plasma membrane (CC). Furthermore, it demonstrated enrichment in identical protein binding (MF). The KEGG pathway analysis provides a modelling tool to illustrate how fundamental molecular or biological processes interact (*Figure 1F*). In our study, the KEGG pathway analysis revealed significant enrichment in vitamin D receptor pathway, PPAR signaling pathway, renin-angiotensin system (RAS) signaling pathway, fatty acids and lipoproteins transport in hepatocytes.

miRNA analysis from online data

Using the limma package, differential expression analysis of miRNAs in the GSE108755 dataset was conducted, identifying 298 differentially expressed miRNAs, with 147 upregulated and 151 downregulated miRNAs at a significance threshold of P<0.05. As there were too many potential targets, we increased the threshold to |logFC| >1, P<0.05 (*Figure 2A*). Using heatmap, we identified 9 significantly upregulated and 22 significantly downregulated miRNAs (*Figure 2B*). Volcano plots and heatmap analyses revealed that hsa-miR-9-5p exhibited the most significant change (logFC =1.276, P=0.02). Cells in both control group and hyperoxia group were harvested and undergone real-time quantitative PCR analysis. Results showed a significant increase in miR-9-5p expression (P<0.001), and thus it was chosen as the candidate gene for further investigation (*Figure 2C-2G*). Using three online miRNA target gene prediction databases—miRDB, miRWalk, and TargetScan—we identified an intersection of 129 target genes (*Figure 2H*). Given that the regulation of ferroptosis is a key factor in the pathogenesis of BPD, we further intersected these 129 target genes with both the BPD DEG set and the ferroptosis gene set, ultimately identifying GCH1 as the sole target gene (*Figure 2I*).

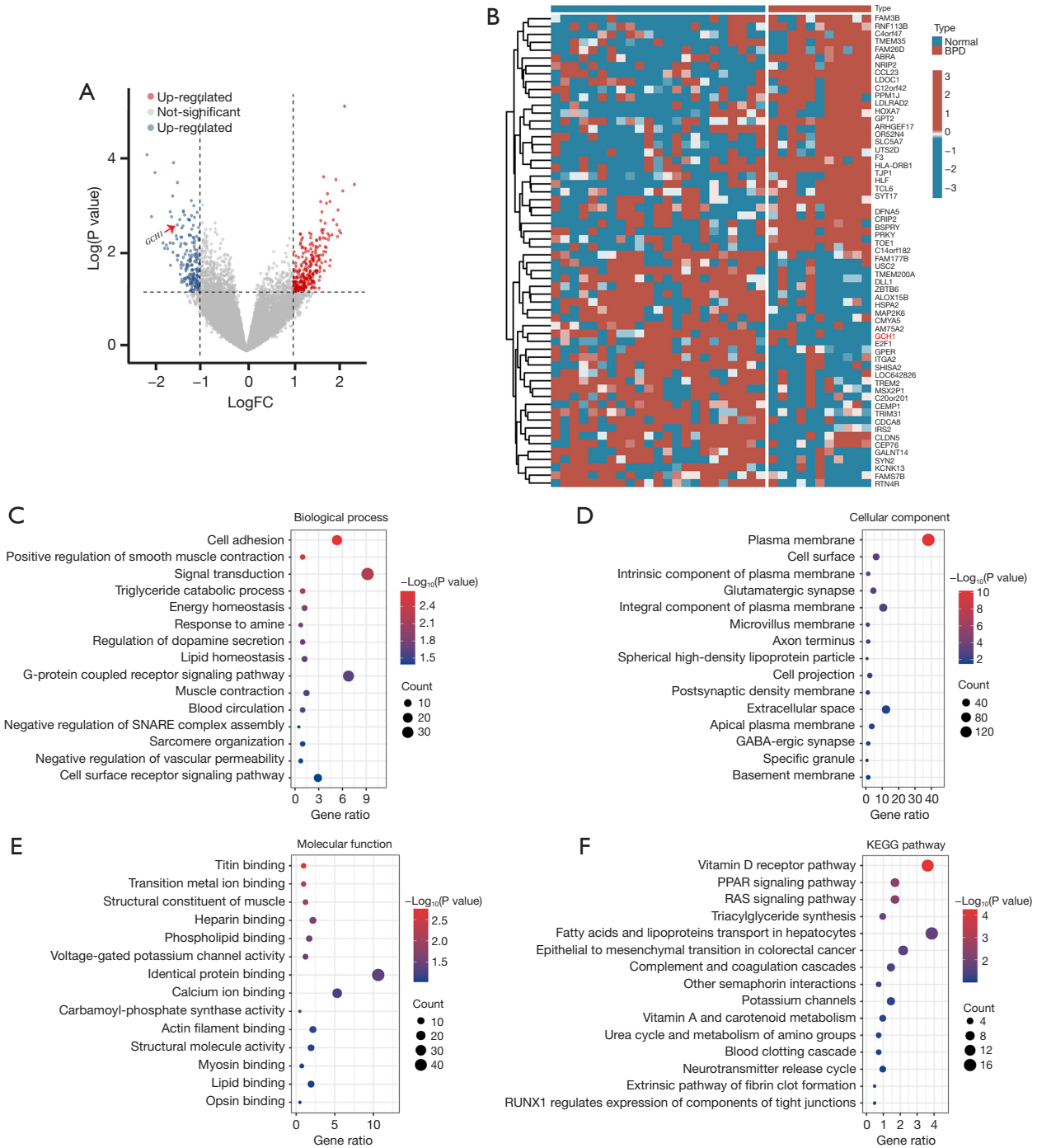

Figure 1 Identification of DGEs for BPD from datasets GSE188944 and GSE108754. (A) Volcano plots of DGEs. Red and blue dots denote significantly upregulated and downregulated values, while gray dots represent genes with no significant difference. (B) Clustered heatmap of DGEs. Red indicates that the DEGs have a high expression value and blue indicates that a DEGs have a low expression value (|logFC| >1, P<0.05). (C) Biological process analysis on DGEs. (D) Cellular component analysis on DGEs. (E) Molecular function analysis on DGEs. (F) KEGG pathway analysis on DGEs. BPD, bronchopulmonary dysplasia; DGEs, differentially expressed genes; FC, fold change; GABA, gamma-Aminobutyric acid; KEGG, Kyoto Encyclopedia of Genes and Genomes.

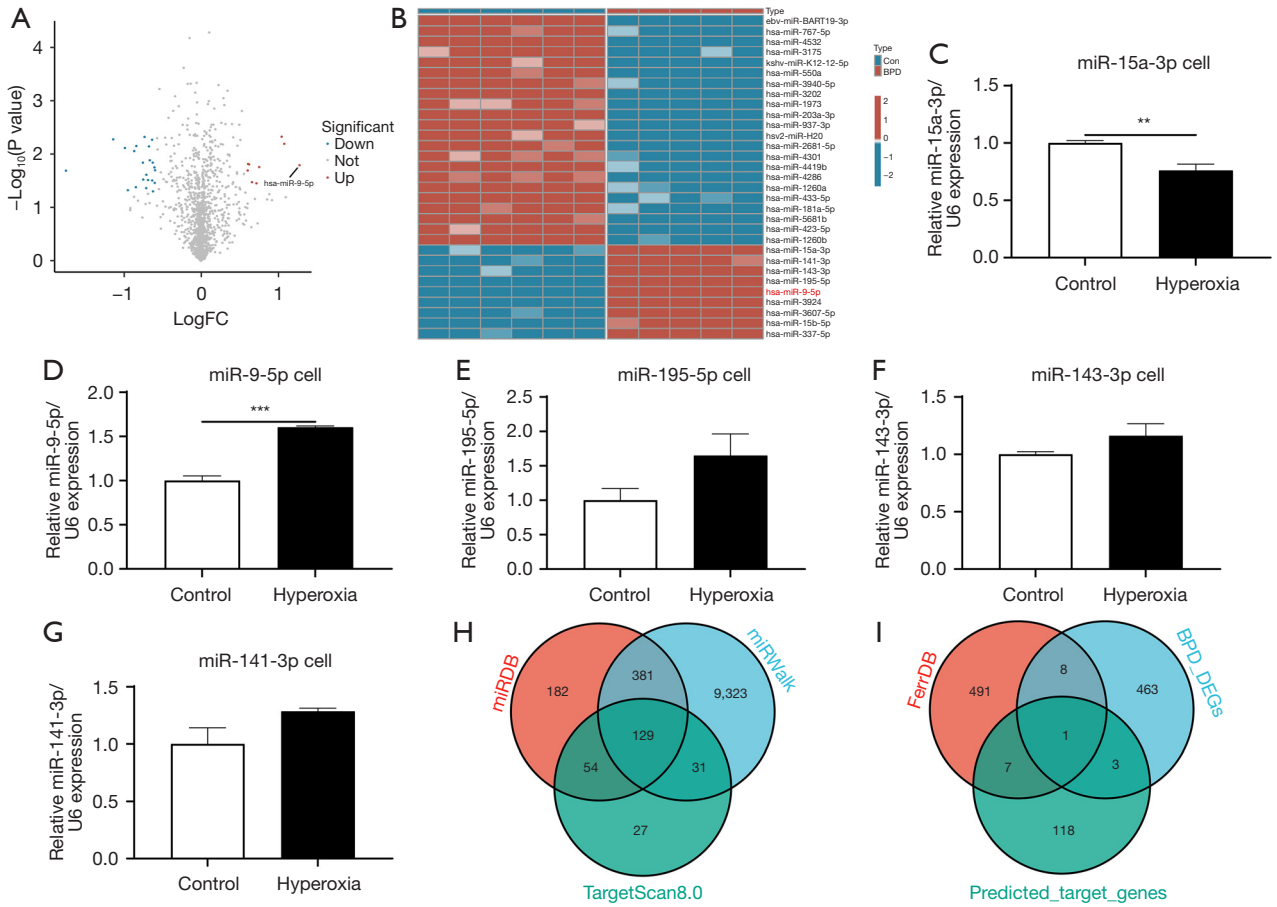

Figure 2 Differentially expressed miRNAs from GSE108755 dataset and identification of miRNA target gene. (A) Volcano plot of 32 differentially expressed miRNAs. The red and blue points symbolize the upregulated and downregulated miRNAs with statistical significance (|logFC| >1, P<0.05). (B) Heatmap analyses revealed that hsa-miR-9-5p exhibited the most significant change (logFC =1.276, P=0.02). (C-G) Real-time quantitative PCR detection of miRNA level changes between the two groups. (H) An intersection of 129 target genes of miR-9-5p from miRDB, miRWalk, and TargetScan 8.0. (I) An intersection of miR-9-5p target genes with the BPD differentially expressed gene set and the ferroptosis gene set. **, P<0.01; ***, P<0.001. BPD, bronchopulmonary dysplasia; DGEs, differentially expressed genes; FC, fold change; miRNA, microRNA; PCR, polymerase chain reaction.

GO and KEGG pathway enrichment analysis of DEGs

Bubble plots for GO functional enrichment analysis and KEGG pathway enrichment of DEGs are shown in *Figure 3A-3C* and *Figure 3D*, respectively. The three ontologies in the GO enrichment analysis are "MF", "CC", and "BP". Further functional enrichment analysis revealed that DEGs are significantly associated with protein binding in MF; with cytosol, cytoplasm, and nucleus in CC; and with the regulation of transcription by RNA polymerase II in BP. KEGG pathway enrichment analysis showed that DEGs are primarily enriched in the cytoskeleton in muscle cells, endocytosis, MAPK signaling pathway, and RAS signaling pathway.

Construction of PPI network and key module screening

For the 129 intersecting predicted target genes, interaction relationships were extracted from the STRING database to construct a PPI network (*Figure 4*). In the interaction results among the predicted target genes, GCH1 formed a major node, suggesting its significant regulatory role in the associated pathophysiological processes.

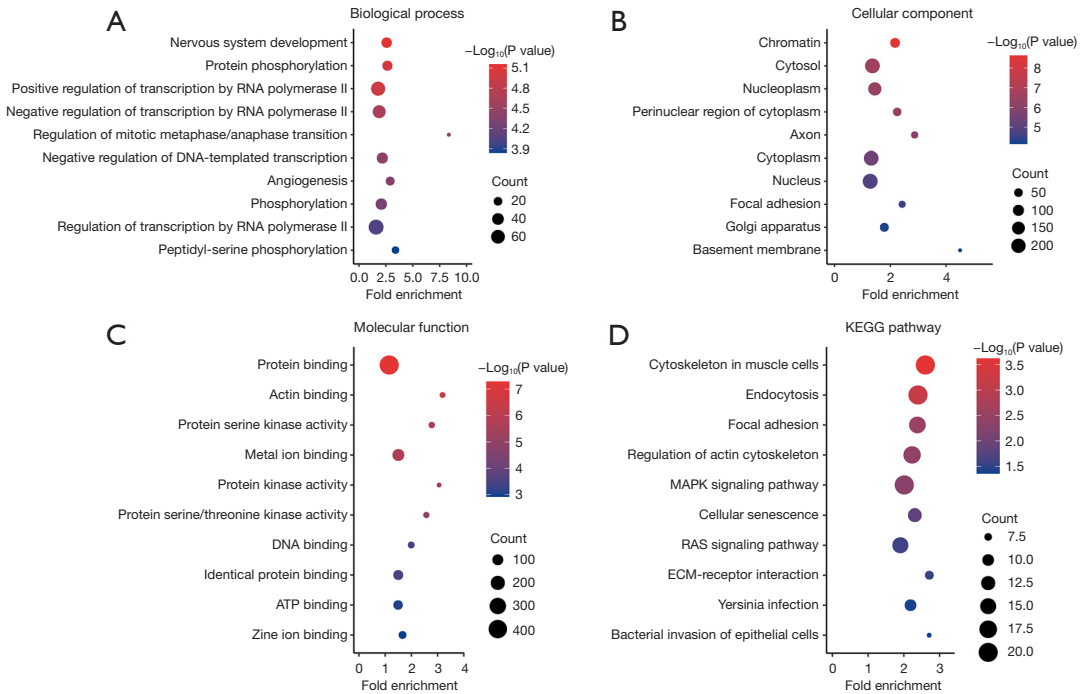

Figure 3 Enrichment analysis of DEGs. Gene Ontology enrichment analysis includes (A) biological process, (B) cellular component, and (C) molecular function. (D) KEGG enrichment analysis of DEGs. ATP, adenosine triphosphate; DGEs, differentially expressed genes; ECM, extracellular matrix; KEGG, Kyoto Encyclopedia of Genes and Genomes.

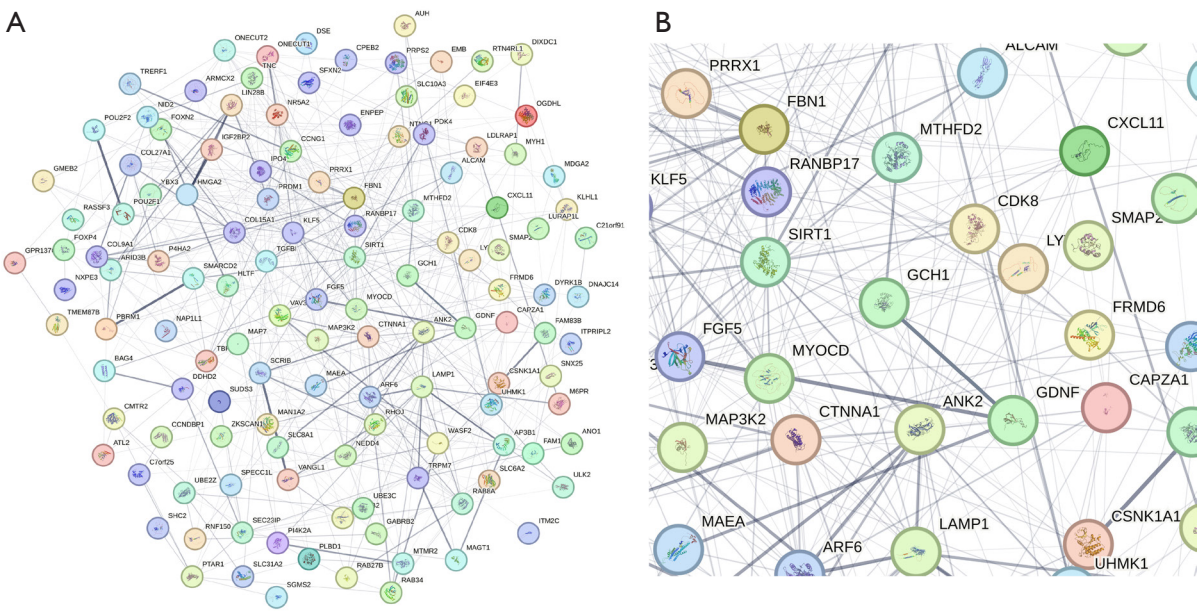

Figure 4 PPI network of predicted target genes. Node size represents the degree of each node, with larger nodes indicating a higher number of connections (A,B). PPI, protein-protein interaction.

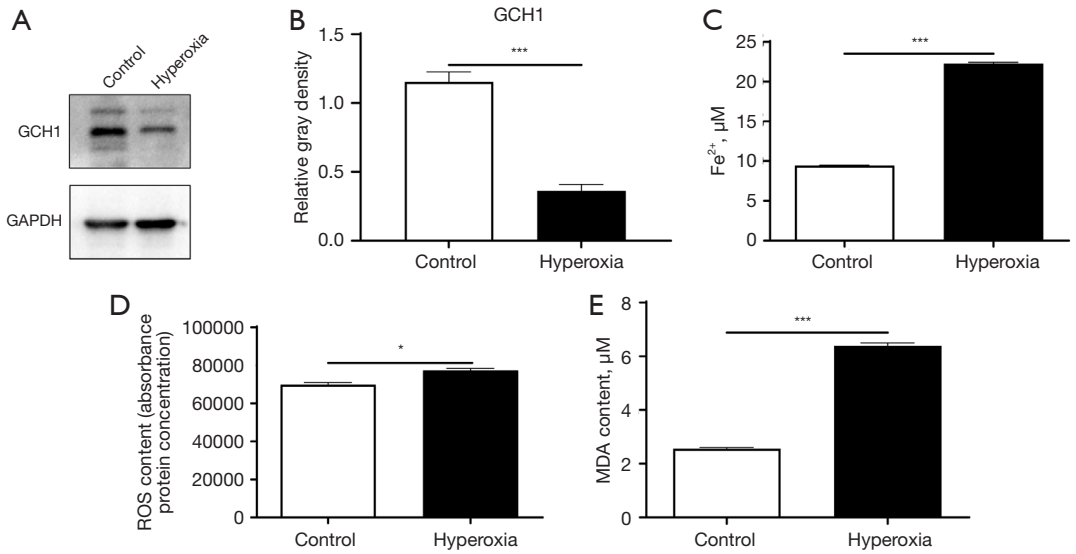

Figure 5 Expression levels of miR-9-5p, GCH1, Fe^{2+}, ROS, and MDA in both cell groups. (A) Western blot analysis showing changes in GCH1 translation levels between the two cell groups. (B) Gray value analysis of western blot bands from panel A. Each experiment was repeated three times. (C) Fe^{2+} levels in both cell groups. Each experiment was repeated five times. (D) ROS expression levels in both cell groups. Each experiment was repeated five times. (E) MDA expression levels in both cell groups. Each experiment was repeated five times. *, P=0.007; ***, P<0.001. GCH1, guanosine triphosphate cyclohydrolase 1; MDA, malondialdehyde; ROS, reactive oxygen species.

Expression of GCH1, ferrous ions, ROS, and MDA in both cell groups

The translational variations of GCH1 in control cells and hyperoxia ones were detected by western blot, and results showed a marked decrease in GCH1 expression in the hyperoxia-induced injury group (P<0.001). Additionally, Fe^{2+} (P<0.001), ROS (P=0.007) and MDA (P<0.001) levels were significantly elevated in the hyperoxia-induced injury cell model (*Figure 5*).

Discussion

BPD is a disease that presents with a number of characteristic features, including arrest of lung development, impaired alveolar capillary development, increased interstitial fibrosis, pulmonary vascular abnormalities, and reduced branching (31,38). However, the pathogenesis of BPD is complex and not fully understood. Given the rising prevalence of BPD, there is an urgent need to elucidate its underlying mechanisms. Recent advancements in gene chip technology have broadened the application of genomics in disease research, providing new approaches for exploring biomarkers and identifying therapeutic targets for BPD (6). As a widespread regulatory factor, miRNAs have been shown to play a critical role in normal and abnormal lung development and are involved in the pathogenesis and progression of BPD (33,39).

The MLE12 cell line was selected for the hyperoxia-induced injury model due to its relevance to pulmonary epithelial biology, responsiveness to oxidative stress, and alignment with BPD pathogenesis. MLE12 cells are a murine lung epithelial cell line derived from mouse lung tissue, representing alveolar epithelial cells. These cells are critical for alveolar development and gas exchange, which are directly impaired in BPD. Lung epithelial cells are primary targets of hyperoxic injury in BPD, making MLE12 cells a physiologically relevant model to study alveolar damage and repair mechanisms. Hyperoxia-induced injury in MLE12 cells recapitulates key BPD hallmarks observed *in vivo*, including oxidative stress (elevated ROS/MDA), ferroptosis (increased Fe^{2+}), and dysregulated miRNA/mRNA expression (e.g., miR-9-5p upregulation and GCH1 downregulation). Previous study has used MLE12 cells or similar lung epithelial lines to model hyperoxic injury, validating their utility in BPD research (26).

In this study, we analyzed 1,461 human miRNAs in the GSE108755 dataset, identifying nine significantly upregulated and 22 significantly downregulated miRNAs. miR-9-5p was selected as a target due to its critical roles

in various physiological functions, such as tumorigenesis, inflammation, and apoptosis. Bioinformatics analysis showed that miR-9-5p was upregulated in BPD, with high expression observed in the hyperoxia-induced injury cells, suggesting that its overexpression may contribute to BPD progression.

To delve into the pathophysiology of these conditions, we conducted GO pathway analyses focusing on BPs, CCs, and MFs. GO enrichment analysis indicated that DEGs are primarily involved in processes such as angiogenesis, protein binding, and metal ion binding, all of which are closely associated with BPD pathogenesis (40). The formation and maturation of pulmonary blood vessels, especially pulmonary microvessels, are critical for alveolar development and structural maintenance. It is widely accepted that vascular development is a key factor influencing the formation of the alveoli (41). Impaired pulmonary vascular development may play a key role in BPD pathogenesis, as inhibition of angiogenesis leads to alveolar simplification in neonatal rodents, resembling the pathology observed in preterm infants with BPD (40).

KEGG pathway analysis revealed key BPD-related pathways, including the MAPK signaling pathway, RAS signaling pathway, and extracellular matrix (ECM)-receptor interactions. These findings are consistent with the established pathophysiological mechanisms of cell proliferation, differentiation, apoptosis, and stress response. The MAPK signaling pathway plays an important role in mediating hyperoxia-induced lung injury (42). It has been demonstrated that exposure to 95% oxygen and H_2O_2 stress activates MAPK family members p38 and JNK, which in turn induce apoptosis and cell damage. Conversely, the specific inhibition of MAPK activation has been shown to improve cell survival (43). This study observed high miR-9-5p expression in the hyperoxia-induced injury cells, suggesting that it may promote BPD progression through pathways such as MAPK signaling. Moreover, the ACE-2/Ang(1–7)/Mas axis in the RAS is associated with acute lung injury, pulmonary hypertension, and pulmonary fibrosis (44). Studies indicate that ACE-2 expression is significantly reduced under hyperoxia (45), and the Mas receptor antagonist A779 can reverse the protective effect of ACE-2 (46,47). Hyperoxia caused high airflow restriction, increased pulmonary expression of the pro-fibrotic RAS pathway, and decreased expression of the pro-developmental in BPD mouse model (48,49). miR-9-5p promotes NF-κB activation in pancreatic cancer and endometriosis by targeting SIRT1, thereby enhancing inflammation and tumor progression, while in traumatic brain injury and systemic lupus erythematosus, it suppresses NF-κB signaling via PTCH1 or direct inhibition of NFKB1, alleviating neuroinflammation and immune dysfunction. This dual role highlights miR-9-5p as a versatile modulator of inflammation, with implications for diverse pathological contexts.

A PPI network analysis was conducted from the STRING database using 129 intersecting predicted target genes. This initiative aimed to gain insights into potential treatment strategies and biomarker discovery for BPD. Among all the nodes, GCH1 formed a major node, suggesting its significant regulatory role in the associated pathophysiological processes.

We then used real-time quantitative PCR to measure the expression levels of miR-9-5p in the control group and the hyperoxia-induced injury group. In osteoarthritis and rheumatoid arthritis, it exerts anti-inflammatory effects by inhibiting pro-inflammatory pathways by targeting syndecan-1 or REST/miR-132 axis. Conversely, in metabolic syndrome and COPD, miR-9-5p may contribute to pro-inflammatory responses by suppressing protective genes like *ABCA1* or interacting with long non-coding RNAs (lncRNAs) to activate NF-κB signaling. These divergent roles highlight the complexity of miR-9-5p's regulatory network across diseases, emphasizing the need for disease-specific mechanistic investigations. We found increased miR-9-5p expression and decreased GCH1 expression in the hyperoxia cells, with concurrent increases in ROS and MDA levels, suggesting that miR-9-5p may play an important role in BPD through ferroptosis by regulating the expression of its downstream target gene, GCH1. GCH1 is the rate-limiting enzyme for BH4 synthesis and inhibits ferroptosis through the GCH1/BH4/DHFR pathway during antioxidation (50). Additionally, caffeine increases GCH1 levels in neonatal rats, raising BH4 concentration to enhance eNOS activity, thereby protecting immature lungs from hyperoxic injury (26). Ferroptosis is a novel iron-dependent programmed cell death characterized by the accumulation of lipid peroxides (50). Studies have shown that GCH1 prevents ferroptosis by increasing BH4 levels and remodeling the lipid membrane environment (32,51). In lipid peroxidation, ROS accumulation is a hallmark of ferroptosis, and MDA, a product of lipid peroxidation, reflects the degree of lipid peroxidation in the body (52,53). In this study, GCH1 expression decreased, while Fe^{2+}, ROS, and MDA levels increased in the hyperoxia-induced injury cell model,

suggesting the presence of ferroptosis in the neonatal mouse BPD model, consistent with previous reports (54,55). Bioinformatics analysis identified GCH1 as a potential target gene of miR-9-5p, consistent with existing literature (56). However, the specific regulatory relationship between miR-9-5p and GCH1 was not explored in-depth in this study. Future experiments, such as luciferase reporter assays and CRISPR knockout models, will be used to investigate its regulatory mechanisms in animal and cell models and in clinical patients.

Conclusions

Through differential expression analysis of the GEO database, this study selected miR-9-5p and GCH1 as research targets and constructed a hyperoxia-induced injury cell model to investigate the expression of miR-9-5p and GCH1 in BPD. This study provides new insights into the molecular mechanisms of BPD, facilitating the identification of potential therapeutic targets. Future research should take the primary human alveolar cells and neonatal mouse models into consideration to further examine the role of miR-9-5p and GCH1 in BPD, providing a theoretical and experimental basis for the diagnosis and treatment of BPD.

Acknowledgments

None.

Footnote

Reporting Checklist: The authors have completed the MDAR reporting checklists. Available at https://tp.amegroups.com/article/view/10.21037/tp-2024-595/rc

Data Sharing Statement: Available at https://tp.amegroups.com/article/view/10.21037/tp-2024-595/dss

Peer Review File: Available at https://tp.amegroups.com/article/view/10.21037/tp-2024-595/prf

Funding: This study was financially supported by the National Natural Science Foundation (NNSF) of China (No. 82271741), Key Project of Medical Research of Jiangsu Provincial Health Commission (No. ZD2021013), Gusu Health Leading Talents (No. GSWS2022055), Clinical Technology High-End Platform and Transformation Base Construction Project (No. ML13101523), and "Suiyuan" Clinical Research Project of Children's Hospital of Soochow University (No. SY003).

Conflicts of Interest: All authors have completed the ICMJE uniform disclosure form (available at https://tp.amegroups.com/article/view/10.21037/tp-2024-595/coif). The authors have no conflicts of interest to declare.

Ethical Statement: The authors are accountable for all aspects of the work in ensuring that questions related to the accuracy or integrity of any part of the work are appropriately investigated and resolved. The study was conducted in accordance with the Declaration of Helsinki and its subsequent amendments.

References

1. Northway WH Jr, Rosan RC, Porter DY. Pulmonary disease following respirator therapy of hyaline-membrane disease. Bronchopulmonary dysplasia. N Engl J Med 1967;276:357-68.
2. Maeda H, Li X, Go H, et al. miRNA Signatures in Bronchopulmonary Dysplasia: Implications for Biomarkers, Pathogenesis, and Therapeutic Options. Front Biosci (Landmark Ed) 2024;29:271.
3. Stoll BJ, Hansen NI, Bell EF, et al. Neonatal outcomes of extremely preterm infants from the NICHD Neonatal Research Network. Pediatrics 2010;126:443-56.
4. Collaborative Study Group for Extremely Preterm and Extremely Low Birth Weight Infants. Short-term outcomes and their related risk factors of extremely preterm and extremely low birth weight infants in Guangdong province. Zhonghua Er Ke Za Zhi 2019;57:934-42.
5. Ambalavanan N, Van Meurs KP, Perritt R, et al. Predictors of death or bronchopulmonary dysplasia in preterm infants with respiratory failure. J Perinatol 2008;28:420-6.
6. Gough A, Linden M, Spence D, et al. Impaired

lung function and health status in adult survivors of bronchopulmonary dysplasia. Eur Respir J 2014;43:808-16.
7. Sun T, Yu HY, Yang M, et al. Risk of asthma in preterm infants with bronchopulmonary dysplasia: a systematic review and meta-analysis. World J Pediatr 2023;19:549-56.
8. Nguyen KL, Fitzgerald DA, Webb A, et al. Neurodevelopmental outcomes of extremely preterm infants with bronchopulmonary dysplasia (BPD) - A retrospective cohort study. Paediatr Respir Rev 2024;50:23-30.
9. McGrath-Morrow SA, Collaco JM. Bronchopulmonary dysplasia: what are its links to COPD? Ther Adv Respir Dis 2019;13:1753466619892492.
10. An N, Li J, Li M. Role of systemic inflammation response index and prognostic nutritional index in the prediction of moderate-to-severe bronchopulmonary dysplasia in very preterm infants. Transl Pediatr 2025;14:52-60.
11. Golshan-Tafti M, Bahrami R, Dastgheib SA, et al. The association between VEGF genetic variations and the risk of bronchopulmonary dysplasia in premature infants: a meta-analysis and systematic review. Front Pediatr 2024;12:1476180.
12. Bartel DP. MicroRNAs: genomics, biogenesis, mechanism, and function. Cell 2004;116:281-97.
13. Lewis BP, Burge CB, Bartel DP. Conserved seed pairing, often flanked by adenosines, indicates that thousands of human genes are microRNA targets. Cell 2005;120:15-20.
14. Ambros V. The functions of animal microRNAs. Nature 2004;431:350-5.
15. Rogers LK, Robbins M, Dakhlallah D, et al. Attenuation of miR-17~92 Cluster in Bronchopulmonary Dysplasia. Ann Am Thorac Soc 2015;12:1506-13.
16. Olave N, Lal CV, Halloran B, et al. Regulation of alveolar septation by microRNA-489. Am J Physiol Lung Cell Mol Physiol 2016;310:L476-87.
17. Ruiz-Camp J, Quantius J, Lignelli E, et al. Targeting miR-34a/Pdgfra interactions partially corrects alveologenesis in experimental bronchopulmonary dysplasia. EMBO Mol Med 2019;11:e9448.
18. Zhang TX, Duan XC, Cui Y, et al. Clinical significance of miR-9-5p in NSCLC and its relationship with smoking. Front Oncol 2024;14:1376502.
19. Babion I, Jaspers A, van Splunter AP, et al. miR-9-5p Exerts a Dual Role in Cervical Cancer and Targets Transcription Factor TWIST1. Cells 2019;9:65.
20. Chen L, Hu W, Li G, et al. Inhibition of miR-9-5p suppresses prostate cancer progress by targeting StarD13. Cell Mol Biol Lett 2019;24:20.
21. Wu J, He J, Tian X, et al. microRNA-9-5p alleviates blood-brain barrier damage and neuroinflammation after traumatic brain injury. J Neurochem 2020;153:710-26.
22. Zhao Y, Li T, Jiang Z, et al. The miR-9-5p/CXCL11 pathway is a key target of hydrogen sulfide-mediated inhibition of neuroinflammation in hypoxic ischemic brain injury. Neural Regen Res 2024;19:1084-94.
23. Zhou C, Gao Y, Ding P, et al. The role of CXCL family members in different diseases. Cell Death Discov 2023;9:212.
24. Fanet H, Capuron L, Castanon N, et al. Tetrahydrobioterin (BH4) Pathway: From Metabolism to Neuropsychiatry. Curr Neuropharmacol 2021;19:591-609.
25. Lignelli E, Palumbo F, Myti D, et al. Recent advances in our understanding of the mechanisms of lung alveolarization and bronchopulmonary dysplasia. Am J Physiol Lung Cell Mol Physiol 2019;317:L832-87.
26. Jing X, Huang YW, Jarzembowski J, et al. Caffeine ameliorates hyperoxia-induced lung injury by protecting GCH1 function in neonatal rat pups. Pediatr Res 2017;82:483-9.
27. Chen W, Zheng D, Yang C. The Emerging Roles of Ferroptosis in Neonatal Diseases. J Inflamm Res 2023;16:2661-74.
28. Zhang J, Zheng Y, Wang Y, et al. YAP1 alleviates sepsis-induced acute lung injury via inhibiting ferritinophagy-mediated ferroptosis. Front Immunol 2022;13:884362.
29. Zhang Z, Chen K, Pan D, et al. A predictive model for preterm infants with bronchopulmonary dysplasia based on ferroptosis-related lncRNAs. BMC Pulm Med 2023;23:367.
30. Deng X, Bao Z, Yang X, et al. Molecular mechanisms of cell death in bronchopulmonary dysplasia. Apoptosis 2023;28:39-54.
31. Luo Y, Zhang Z, Xi S, et al. Bioinformatics analyses and experimental validation of ferroptosis-related genes in bronchopulmonary dysplasia pathogenesis. PLoS One 2024;19:e0291583.
32. Kraft VAN, Bezjian CT, Pfeiffer S, et al. GTP Cyclohydrolase 1/Tetrahydrobiopterin Counteract Ferroptosis through Lipid Remodeling. ACS Cent Sci 2020;6:41-53.
33. Albertson DG, Pinkel D. Genomic microarrays in human genetic disease and cancer. Hum Mol Genet 2003;12 Spec No 2:R145-52.
34. Valadie CT, Arya S, Arora T, et al. A bioinformatics approach towards bronchopulmonary dysplasia. Transl Pediatr 2023;12:1213-24.

35. Zhang X, Peng W, Zhang S, et al. MicroRNA expression profile in hyperoxia-exposed newborn mice during the development of bronchopulmonary dysplasia. Respir Care 2011;56:1009-15.
36. Wang C, Zhang S, Zhu L, et al. Integrated MicroRNA-mRNA Analyses of Distinct Expression Profiles in Hyperoxia-Induced Bronchopulmonary Dysplasia in Neonatal Mice. Am J Perinatol 2022;39:1702-10.
37. Wang Y, Wang X, Xu Q, et al. CircRNA, lncRNA, and mRNA profiles of umbilical cord blood exosomes from preterm newborns showing bronchopulmonary dysplasia. Eur J Pediatr 2022;181:3345-65.
38. Zou Z, Li Y, Liu J, et al. Identification and Validation of Oxidative Stress-Related Biomarkers for Bronchopulmonary Dysplasia. Mol Biotechnol 2024. [Epub ahead of print]. doi: 10.1007/s12033-024-01281-9.
39. Xu F, Mei Y, Zhang Y, et al. Pathogenesis of bronchopulmonary dysplasia in preterm neonates revealed by an RNA sequencing interaction network analysis. Transl Pediatr 2022;11:2004-15.
40. Durlak W, Thébaud B. The vascular phenotype of BPD: new basic science insights-new precision medicine approaches. Pediatr Res 2024;96:1162-71.
41. Baker CD, Abman SH. Impaired pulmonary vascular development in bronchopulmonary dysplasia. Neonatology 2015;107:344-51.
42. Romashko J 3rd, Horowitz S, Franek WR, et al. MAPK pathways mediate hyperoxia-induced oncotic cell death in lung epithelial cells. Free Radic Biol Med 2003;35:978-93.
43. Averill-Bates D. Reactive oxygen species and cell signaling. Review. Biochim Biophys Acta Mol Cell Res 2024;1871:119573.
44. Zhang PX, Han CH, Zhou FJ, et al. Renin-angiotensin system and its role in hyperoxic acute lung injury. Undersea Hyperb Med 2016;43:239-46.
45. Oarhe CI, Dang V, Dang M, et al. Hyperoxia downregulates angiotensin-converting enzyme-2 in human fetal lung fibroblasts. Pediatr Res 2015;77:656-62.
46. Mohamed T, Abdul-Hafez A, Uhal BD. Regulation of ACE-2 enzyme by hyperoxia in lung epithelial cells by post-translational modification. J Lung Pulm Respir Res 2021;8:47-52.
47. Li Y, Cao Y, Zeng Z, et al. Angiotensin-converting enzyme 2/angiotensin-(1-7)/Mas axis prevents lipopolysaccharide-induced apoptosis of pulmonary microvascular endothelial cells by inhibiting JNK/NF-κB pathways. Sci Rep 2015;5:8209.
48. Dowell J, Bice Z, Yan K, et al. Hyperoxia-induced airflow restriction and Renin-Angiotensin System expression in a bronchopulmonary dysplasia mouse model. Physiol Rep 2024;12:e15895.
49. Giusto K, Wanczyk H, Jensen T, et al. Hyperoxia-induced bronchopulmonary dysplasia: better models for better therapies. Dis Model Mech 2021;14:dmm047753.
50. Liu X, Zhang J, Xie W. The role of ferroptosis in acute lung injury. Mol Cell Biochem 2022;477:1453-61.
51. Wang D, Liang W, Huo D, et al. SPY1 inhibits neuronal ferroptosis in amyotrophic lateral sclerosis by reducing lipid peroxidation through regulation of GCH1 and TFR1. Cell Death Differ 2023;30:369-82.
52. Wang B, Wang Y, Zhang J, et al. ROS-induced lipid peroxidation modulates cell death outcome: mechanisms behind apoptosis, autophagy, and ferroptosis. Arch Toxicol 2023;97:1439-51.
53. Rochette L, Dogon G, Rigal E, et al. Lipid Peroxidation and Iron Metabolism: Two Corner Stones in the Homeostasis Control of Ferroptosis. Int J Mol Sci 2022;24:449.
54. Jia D, Zheng J, Zhou Y, et al. Ferroptosis is Involved in Hyperoxic Lung Injury in Neonatal Rats. J Inflamm Res 2021;14:5393-401.
55. Lan J, Chen X, Xu F, et al. Self-assembled miR-134-5p inhibitor nanoparticles ameliorate experimental bronchopulmonary dysplasia (BPD) via suppressing ferroptosis. Mikrochim Acta 2023;190:491.
56. Jia S, Chen G, Liang Y, et al. GCH1-regulated miRNAs are potential targets for microglial activation in neuropathic pain. Biosci Rep 2021;41:BSR20210051.

Cite this article as: Zhang X, Zhu L, Wang H, Hu J, Huo J, He S, Shen Y, Zhu X. Screening for biomarkers of bronchopulmonary dysplasia: a bioinformatics analysis. Transl Pediatr 2025;14(4):658-670. doi: 10.21037/tp-2024-595